

Dynamic response of a repaired composite beam with an adhesively bonded patch under a harmonic peeling load

A. Vaziri¹, H. Nayeb-Hashemi*

Department of Mechanical, Industrial and Manufacturing Engineering, Northeastern University, Boston, MA 02115, USA

Accepted 11 May 2005

Available online 21 July 2005

Abstract

The dynamic response of repaired composite beams under a harmonic peeling load was studied theoretically and experimentally. The repair method was based on removal of the damaged region and bonding a composite patch into the gap with adhesive. In the theoretical part, the equations of motion in the axial and transverse directions were derived assuming that the viscoelastic adhesive layer resists both peeling and shear stresses and both the patch and parent materials behave as Euler–Bernouli beams. The validity of the theoretical model for evaluating the dynamic response of repaired composite beams was examined with the results of the finite element model. The finite element results indicated that the deformation mechanism of the repaired composite beam depends on the adhesive elastic modulus. For low values of the adhesive elastic modulus, shear deformation in the adhesive layer is the dominant deformation mechanism and the proposed theoretical model replicated the results of the computational analysis.

In the experimental part, the response of unidirectional fiberglass-reinforced epoxy composite specimens with various repaired patch lengths, thickness, and material properties were measured by hammer test technique using a non-contact laser vibrometer. The patch section was either the fiberglass-reinforced epoxy composite or E-glass fiber reinforced composites with various stacking sequences. The repairing patches were bonded to the composite beam with an epoxy. The experimental results were compared to those of the theoretical model and finite element analyses. The experimental results were related to the adhesive material properties, its loss factor and to the patch material properties.

© 2005 Elsevier Ltd. All rights reserved.

Keywords: Composite materials; Adhesive; Patch; Dynamic response

1. Introduction

Damages of various types often initiate and propagate in components made of fiber-reinforced composite materials during their service life. The presence of the damage results in degradation of the component mechanical properties (i.e. stiffness and fatigue properties) and increases its damping [1–3]. To assure structural integrity, damaged structural components

should be replaced or repaired. However in many cases, the replacement of these components is impossible or costly. Consequently, composite repair has developed into an important technology to restore the strength, stiffness and durability of the damaged components [4]. The repair method depends on the extent of damage and certification requirements. Repair of the damage can be in form of bolted or/and adhesively bonded patching [5,6] or resin injection [7,8] into the damaged area.

There are mainly two types of patch configuration available for repair of the composite components, the overlap joint (external patching) and scarf patching (which involves removal of the damaged region and re-consolidation of the composite structure into the gap) [9,10]. The externally bonded composite patch is an

*Corresponding author. Tel.: +1 617 373 5515;
fax: +1 617 373 2921.

E-mail address: hamid@coe.neu.edu (H. Nayeb-Hashemi).

¹Current address: Division of Engineering and Applied Sciences, Harvard University, Cambridge, MA 02138, USA.

Nomenclature

A_i	cross-section area of i th region
E_a	elastic modulus of adhesive
$F(t)$	applied peeling load
G	complex shear modulus of adhesive
G_0	real part of the adhesive shear modulus
H_0	adhesive thickness
h_i	thickness of i th region
k	stiffness per unit length of the adhesive

l_i	length of i th region
L	overall length of the composite beam
u_i	axial displacement of i th region
\bar{u}_i	normalized axial displacement of i th region
y_i	transverse displacement of i th region
\bar{y}_i	normalized transverse displacement of i th region
w	composite beam width
τ	shear stress
η	adhesive loss factor
ρ	density of i th region
ω	peeling load frequency

effective method of repairing cracked and damaged components. The main advantage of an external patch is its simplicity to manufacture and apply. However, this method alters the aerodynamic contour of the component if the patch is thick. In addition, the studies on adhesively bonded lap joints under static [11–14] and dynamic loadings [15–17] indicated that both maximum shear and peel stresses are developed at the joint edges, while the middle of the joint carries very little shear or peel stress. In contrast to the external patch, an internal patch results in minor aerodynamic contour changes, while offering better stress distribution along the bond. In addition, removing the damage part may be essential in the case of widespread cracking [18].

Internal or external composite patches can be bonded to the parent structure with bolts and/or adhesive. The major disadvantage of a bolted patch repair is the stress concentration in the region of the bolt holes. In contrast, adhesive bonding of the repair patch is the most common method due to the advantages that it offers, such as lightness in weight, ease of manufacturing, and more uniform stress distribution along the joint in comparison to a bolted patch. Other advantages of adhesive bonding include corrosion resistance, cost-effective manufacturing, better strain accommodation, and better appearance. In addition, adhesively bonded composite patches have been shown to provide high levels of bond durability under operating conditions.

Despite the many advantages that adhesively bonded patches offer, adhesive bonding is often applied with caution. There are relatively few studies related to the short-term and long-term performances of repaired composite components or composite patches under static and dynamic loading. Some studies focus on metal components repaired with composite patches [2,19–22], others examine composite components repaired with metal patches [23–25], and still others investigate composite components repaired with composite patches [4,25–27]. Of these, only Refs. [2,26,27]

dealt with vibrational behavior. Furthermore, the dynamic behavior of adhesively bonded joints with various geometries is explored in [28–31].

The objective of the work reported in this paper was to understand the effect of patch repair constituents on the dynamic response of repaired composite beams (with adhesively bonded internal repair patch). A theoretical investigation for evaluating the dynamic response of a repaired composite beam subjected to a harmonic peeling load is presented in Section 2. Section 3 presents the experimental procedure utilized to obtain the vibrational characteristics of the repaired composite beams is presented. In Section 4, the results of the theoretical and experimental investigations are compared for various configurations of repaired composite beams. Finite element analysis is performed to explore the discrepancy between the theoretical and experimental results. A limited parametric study is conducted in order to gain some insight into the effect of the adhesive mechanical properties on the deformation field of the repair region of the composite beam under the dynamic loading.

2. Theoretical investigations

Fig. 1 shows a schematic diagram of a clamped repaired composite beam with an adhesively bonded composite patch, subjected to a harmonic peeling load, $F(t)$, at its free end. The axial and transverse dynamic responses of the system are obtained by dividing the repaired composite beam into four regions, as shown in Fig. 1. The adhesive is assumed to be viscoelastic material with shear modulus $G = G_0(1 + i\eta)$, where η is the adhesive loss factor and G_0 is the real part of the adhesive shear modulus. Furthermore, the adhesive is assumed to be an elastic foundation resisting both peeling stress and shear stress. The peel stress can be presented as $k(y_i - y_j)$, where k is the stiffness of the

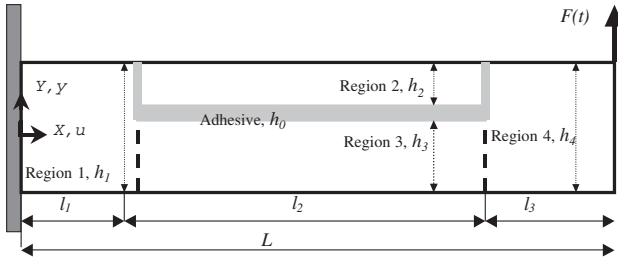


Fig. 1. Schematic model of a repaired composite beam with an internal adhesively bonded patch.

elastic foundation and y_i and y_j are transverse displacements of the regions. The stiffness of the elastic foundation can be presented as $k = (E_a w / h_0)$, where E_a is the elastic modulus of the adhesive, w is the width of the overlap and h_0 is the adhesive thickness. Furthermore, considering axial and transverse displacements of Regions 2 and 3, the shear stress in the adhesive layer can be expressed as [31]

$$\tau = \frac{G}{2h_0} \left[2u_2 - 2u_3 + h_2 \frac{\partial y_2}{\partial x} + h_3 \frac{\partial y_3}{\partial x} \right], \tag{1}$$

Where h_2 and h_3 are the thickness of the composite adherends (patch and the parent beam) in Regions 2 and 3, and y_2, y_3, u_2 and u_3 are the axial and transverse displacements of corresponding adherends (Fig. 1).

The equation of motions in the axial and transverse direction for the four regions of the repaired composite beam (Fig. 1) are derived in the next section, while the corresponding boundary and continuity equations are presented in Section 2.2.

2.1. Equations of motion in the axial and transverse direction for the regions of the repaired composite beam

A free body diagram of an element in Region 2 is presented in Fig. 2. The relation between the internal forces and moments and the axial and transverse displacements can be presented as

$$\frac{\partial V_2}{\partial x} + (\rho A)_2 \ddot{y}_2 + k(y_2 - y_3) = 0, \tag{2}$$

$$V_2 - \frac{\partial M_{x2}}{\partial x} + \tau w \frac{h_2}{2} = 0, \tag{3}$$

$$\frac{\partial N_{x2}}{\partial x} - \tau w = (\rho A)_2 \ddot{u}_2, \tag{4}$$

where $(\rho A)_i$ is the density \times area of the i th region. N_{xi} and V_i are the internal axial and shear force, respectively, and M_{xi} is the internal moment in the i th region.

A similar approach for an element in Region 3 results in

$$\frac{\partial V_3}{\partial x} + (\rho A)_3 \ddot{y}_3 + k(y_3 - y_2) = 0, \tag{5}$$

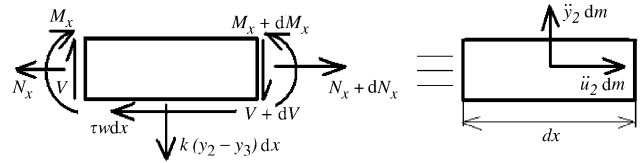


Fig. 2. Free body diagram of an element in Region 2.

$$V_3 - \frac{\partial M_{x3}}{\partial x} + \tau w \frac{h_3}{2} = 0, \tag{6}$$

$$\frac{\partial N_{x3}}{\partial x} + \tau w = (\rho A)_3 \ddot{u}_3. \tag{7}$$

The internal bending moment and axial load can be related to the axial and transverse displacements in each region using the classical laminate theory as

$$N_{xi} = (A_{11})_i \frac{\partial u_i}{\partial x} + (B_{11})_i \frac{\partial^2 y_i}{\partial x^2}, \quad \text{where } i = 1-4, \tag{8}$$

$$M_{xi} = (B_{11})_i \frac{\partial u_i}{\partial x} + (D_{11})_i \frac{\partial^2 y_i}{\partial x^2}, \quad \text{where } i = 1-4, \tag{9}$$

where $(A_{11})_i, (B_{11})_i$ and $(D_{11})_i$ are laminate extensional stiffness, coupling stiffness and bending stiffness of the i th region, respectively.

Substituting for the internal shear force, V_2 , from Eq. (3) into Eq. (2) and using the classical laminate theory for the internal moment, M_{x2} , Eq. (9), the equation of motion in the transverse direction for the element depicted in Fig. 2 can be presented as

$$(\rho A)_2 \ddot{y}_2 + k(y_2 - y_3) + (B_{11})_2 \frac{\partial^3 u_2}{\partial x^3} + (D_{11})_2 \frac{\partial^4 y_2}{\partial x^4} - w \frac{h_2}{2} \frac{\partial \tau}{\partial x} = 0, \tag{10}$$

the same approach for Eqs. (8) and (9) results in

$$(\rho A)_3 \ddot{y}_3 + k(y_3 - y_2) + (B_{11})_3 \frac{\partial^3 u_3}{\partial x^3} + (D_{11})_3 \frac{\partial^4 y_3}{\partial x^4} - w \frac{h_3}{2} \frac{\partial \tau}{\partial x} = 0. \tag{11}$$

By substituting for the shear stress from Eq. (1), Eqs. (10) and (11) can be represented as,

$$\begin{aligned} \text{Region 2 : } & (B_{11})_2 \frac{\partial^3 u_2}{\partial x^3} + (D_{11})_2 \frac{\partial^4 y_2}{\partial x^4} + (\rho A)_2 \ddot{y}_2 + k(y_2 - y_3) \\ & - \frac{wh_2 G}{4h_0} \left(2 \frac{\partial u_2}{\partial x} - 2 \frac{\partial u_3}{\partial x} + h_2 \frac{\partial^2 y_2}{\partial x^2} + h_3 \frac{\partial^2 y_3}{\partial x^2} \right) = 0. \end{aligned} \tag{12}$$

$$\begin{aligned} \text{Region 3 : } & (B_{11})_3 \frac{\partial^3 u_3}{\partial x^3} + (D_{11})_3 \frac{\partial^4 y_3}{\partial x^4} + (\rho A)_3 \ddot{y}_3 + k(y_3 - y_2) \\ & - \frac{wh_3 G}{4h_0} \left(2 \frac{\partial u_2}{\partial x} - 2 \frac{\partial u_3}{\partial x} + h_2 \frac{\partial^2 y_2}{\partial x^2} + h_3 \frac{\partial^2 y_3}{\partial x^2} \right) = 0. \end{aligned} \tag{13}$$

Furthermore, by substituting for the internal axial load Eq. (8), Eqs. (4) and (7) can be represented as

$$\begin{aligned} \text{Region 2 : } & (A_{11})_2 \frac{\partial^2 u_2}{\partial x^2} + (B_{11})_2 \frac{\partial^3 y_2}{\partial x^3} - (\rho A)_2 \ddot{u}_2 \\ & - \frac{wG}{h_0} (u_2 - u_3 + \frac{h_2}{2} \frac{\partial y_2}{\partial x} + \frac{h_3}{2} \frac{\partial y_3}{\partial x}) = 0, \end{aligned} \tag{14}$$

$$\begin{aligned} \text{Region 3 : } & (A_{11})_3 \frac{\partial^2 u_3}{\partial x^2} + (B_{11})_3 \frac{\partial^3 y_3}{\partial x^3} - (\rho A)_3 \ddot{u}_3 \\ & + \frac{wG}{h_0} (u_2 - u_3 + \frac{h_2}{2} \frac{\partial y_2}{\partial x} + \frac{h_3}{2} \frac{\partial y_3}{\partial x}) = 0. \end{aligned} \tag{15}$$

The equations of motions for Regions 1 and 4 are those of classical Euler-Bernouli beam. By substituting for the internal moment and axial load from Eqs. (8) and (9), the equations of motions in the axial and transverse directions for the Regions 1 and 4 can be presented as

$$\text{Region 1 : } (B_{11})_1 \frac{\partial^3 u_1}{\partial x^3} + (D_{11})_1 \frac{\partial^4 y_1}{\partial x^4} + (\rho A)_1 \ddot{y}_1 = 0, \tag{16}$$

$$\text{Region 1 : } (A_{11})_1 \frac{\partial^2 u_1}{\partial x^2} + (B_{11})_1 \frac{\partial^3 y_1}{\partial x^3} - (\rho A)_1 \ddot{u}_1 = 0, \tag{17}$$

$$\text{Region 4 : } (A_{11})_4 \frac{\partial^2 u_4}{\partial x^2} + (B_{11})_4 \frac{\partial^3 y_4}{\partial x^3} - (\rho A)_4 \ddot{u}_4 = 0, \tag{18}$$

$$\text{Region 4 : } (B_{11})_4 \frac{\partial^3 u_4}{\partial x^3} + (D_{11})_4 \frac{\partial^4 y_4}{\partial x^4} + (\rho A)_4 \ddot{y}_4 = 0. \tag{19}$$

For the applied harmonic peeling force of $Fe^{i\omega t}$ at the composite beam free end, the displacement field for each region can be presented as

$$y_j(x, t) = y_j(x)e^{i\omega t}, \quad \text{where } j = 1-4. \tag{20}$$

$$u_j(x, t) = u_j(x)e^{i\omega t}, \quad \text{where } j = 1-4. \tag{21}$$

The dimensionless parameters are defined as

$$b_j = \frac{(B_{11})_j h_1}{2(D_{11})_j}, \quad \text{where } j = 1-4, \tag{22}$$

$$c_j = \frac{2(B_{11})_j}{h_1(A_{11})_j}, \quad \text{where } j = 1-4, \tag{23}$$

$$d_j = -\frac{(\rho A)_j \omega^2 L^4}{(D_{11})_j}, \quad \text{where } j = 1-4, \tag{24}$$

$$e_j = \frac{(\rho A)_j \omega^2 L^2}{(A_{11})_j}, \quad \text{where } j = 1-4, \tag{25}$$

$$a_1 = \frac{kL^4}{(D_{11})_2}, \tag{26}$$

$$a_2 = \frac{G_0}{(D_{11})_2} \frac{wh_2^2 L^2}{4h_0} (1 + i\eta), \tag{27}$$

$$a_3 = \frac{G_0}{(D_{11})_2} \frac{wh_2 h_3 L^2}{4h_0} (1 + i\eta), \tag{28}$$

$$a_4 = \frac{kL^4}{(D_{11})_3}, \tag{29}$$

$$a_5 = \frac{G_0}{(D_{11})_3} \frac{wh_2 h_3 L^2}{4h_0} (1 + i\eta), \tag{30}$$

$$a_6 = \frac{G_0}{(D_{11})_3} \frac{wh_3^2 L^2}{4h_0} (1 + i\eta), \tag{31}$$

$$a_7 = \frac{G_0}{(A_{11})_2} \frac{wL^2}{h_0} (1 + i\eta), \tag{32}$$

$$a_8 = \frac{G_0}{(A_{11})_2} \frac{wh_3 L^2}{h_0 h_2} (1 + i\eta), \tag{33}$$

$$a_9 = \frac{G_0}{(A_{11})_3} \frac{wL^2}{h_0} (1 + i\eta), \tag{34}$$

$$a_{10} = \frac{G_0}{(A_{11})_3} \frac{wh_3 L^2}{h_0 h_2} (1 + i\eta), \tag{35}$$

$$\bar{y}_i = y_i/h_1, \tag{36}$$

$$\bar{u}_i = u_i/(h_1^2/2L) \tag{37}$$

$$\zeta = \frac{x}{L} \quad \text{and} \quad \zeta_1 = \frac{l_1}{L} \quad \text{and} \quad \zeta_2 = \frac{l_1 + l_2}{L}, \tag{38}$$

$$\text{where } L = l_1 + l_2 + l_3. \tag{39}$$

Incorporating the above dimensionless parameters into equations of motions (Eqs. (12)–(19)) results in

$$\text{Region 1 : } \frac{\partial^4 \bar{y}_1}{\partial \zeta^4} + d_1 \bar{y}_1 + b_1 \frac{\partial^3 \bar{u}_1}{\partial \zeta^3} = 0. \tag{40}$$

$$\text{Region 1 : } \frac{\partial^2 \bar{u}_1}{\partial \zeta^2} + e_1 \bar{u}_1 + c_1 \frac{\partial^3 \bar{y}_1}{\partial \zeta^3} = 0. \tag{41}$$

$$\begin{aligned} \text{Region 2 : } & \frac{\partial^4 \bar{y}_2}{\partial \zeta^4} + d_2 \bar{y}_2 + b_2 \frac{\partial^3 \bar{u}_2}{\partial \zeta^3} + a_1 (\bar{y}_2 - \bar{y}_3) \\ & - a_2 \frac{\partial^2 \bar{y}_2}{\partial \zeta^2} - a_3 \frac{\partial^2 \bar{y}_3}{\partial \zeta^2} - a_2 \frac{\partial \bar{u}_2}{\partial \zeta} \\ & + a_2 \frac{\partial \bar{u}_3}{\partial \zeta} = 0. \end{aligned} \tag{42}$$

$$\begin{aligned} \text{Region 2 : } & \frac{\partial^2 \bar{u}_2}{\partial \zeta^2} + e_2 \bar{u}_2 + c_2 \frac{\partial^3 \bar{y}_2}{\partial \zeta^3} - a_8 \frac{\partial \bar{y}_3}{\partial \zeta} \\ & - a_7 (\bar{u}_2 - \bar{u}_3 + \frac{\partial \bar{y}_2}{\partial \zeta}) = 0. \end{aligned} \tag{43}$$

$$\begin{aligned} \text{Region 3 : } & \frac{\partial^4 \bar{y}_3}{\partial \zeta^4} + d_3 \bar{y}_3 + b_3 \frac{\partial^3 \bar{u}_3}{\partial \zeta^3} + a_4 (\bar{y}_3 - \bar{y}_2) \\ & - a_5 \frac{\partial^2 \bar{y}_2}{\partial \zeta^2} - a_6 \frac{\partial^2 \bar{y}_3}{\partial \zeta^2} - a_5 \frac{\partial \bar{u}_2}{\partial \zeta} + a_5 \frac{\partial \bar{u}_3}{\partial \zeta} = 0. \end{aligned} \tag{44}$$

$$\begin{aligned} \text{Region 3 : } & \frac{\partial^2 \bar{u}_3}{\partial \zeta^2} + e_3 \bar{u}_3 + c_3 \frac{\partial^3 \bar{y}_3}{\partial \zeta^3} + a_{10} \frac{\partial \bar{y}_3}{\partial \zeta} \\ & + a_9 (\bar{u}_2 - \bar{u}_3 + \frac{\partial \bar{y}_2}{\partial \zeta}) = 0. \end{aligned} \tag{45}$$

$$\text{Region 4 : } \frac{\partial^2 \bar{u}_4}{\partial \zeta^2} + e_4 \bar{u}_4 + c_4 \frac{\partial^3 \bar{y}_4}{\partial \zeta^3} = 0. \tag{46}$$

$$\text{Region 4 : } \frac{\partial^4 \bar{y}_4}{\partial \zeta^4} + d_4 \bar{y}_4 + b_4 \frac{\partial^3 \bar{u}_4}{\partial \zeta^3} = 0. \tag{47}$$

The solution to Eqs. (40) and (41) is in the form of

$$\bar{y}_1 = \sum_{j=1}^6 A_{1j} e^{S_{1j} \zeta}, \tag{48}$$

$$\bar{u}_i = \sum_{j=1}^6 t_{1j} A_{1j} e^{S_{1j} \zeta}, \tag{49}$$

where S_{1j} ($j = 1-6$) are the roots of the corresponding characteristic equation

$$(c_1 b_1 - 1) S_{1j}^6 - e_1 S_{1j}^4 - d_1 S_{1j}^2 - e_1 d_1 = 0 \tag{50}$$

and

$$t_{1j} = - \frac{S_{1j}^4 + d_1}{b_1 S_{1j}^3} \quad j = 1-6. \tag{51}$$

The solution for the axial and transverse responses of Region 4, Eqs. (46) and (47), are akin to Eqs. (48–51). The solutions for the displacement fields corresponding to Eqs. (42)–(45) can be presented as

$$\begin{aligned} \bar{y}_2 &= \sum_{j=1}^{12} A_{2j} e^{S_j \zeta}, \bar{y}_3 = \sum_{j=1}^{12} t_{2j} A_{2j} e^{S_j \zeta}, \\ \bar{u}_2 &= \sum_{j=1}^{12} t_{3j} A_{2j} e^{S_j \zeta}, \text{ and } \bar{u}_3 = \sum_{j=1}^{12} t_{4j} A_{2j} e^{S_j \zeta}, \end{aligned} \tag{52-55}$$

where S_j ($j = 1-12$) are the roots of the corresponding characteristic equation and t_{ij} ($i = 2-4$ and $j = 1-12$), can be calculated from the governing equations of displacement (the equations are not shown for the sake of brevity).

2.2. Boundary and continuity conditions

The boundary and continuity conditions for the repaired composite beam, Fig. 1, can be expressed as at $x = 0$ (clamped to rigid wall),

$$y_1 = 0, \tag{56}$$

$$\frac{\partial y_1}{\partial x} = 0, \tag{57}$$

$$u_1 = 0, \tag{58}$$

at $x = l_j$:

The transverse displacement and rotation of Regions 1–2 should be equal, which results in

$$y_1 = y_3, \tag{59}$$

$$\frac{\partial y_1}{\partial x} = \frac{\partial y_3}{\partial x}, \tag{60}$$

$$y_1 = y_2, \tag{61}$$

$$\frac{\partial y_1}{\partial x} = \frac{\partial y_2}{\partial x}. \tag{62}$$

Furthermore, the relation between the axial displacements at the boundary of the corresponding regions can be presented as

$$u_2 = u_1 - \left(\frac{h_1 - h_2}{2}\right) \frac{\partial y_1}{\partial x}, \tag{63}$$

$$u_3 = u_1 + \left(\frac{h_1 - h_3}{2}\right) \frac{\partial y_1}{\partial x}. \tag{64}$$

In addition, the force and moment balance at the boundary of each of regions can be presented as,

Force balance in the transverse direction:

$$\begin{aligned} (B_{11})_1 \frac{\partial^2 u_1}{\partial x^2} + (D_{11})_1 \frac{\partial^3 y_1}{\partial x^3} \\ = (D_{11})_2 \frac{\partial^3 y_2}{\partial x^3} + (B_{11})_2 \frac{\partial^2 u_2}{\partial x^2} - \frac{wh_2 G}{4h_0} \\ \times \left(2 \frac{\partial u_2}{\partial x} - 2 \frac{\partial u_3}{\partial x} + h_2 \frac{\partial^2 y_2}{\partial x^2} + h_3 \frac{\partial^2 y_3}{\partial x^2} \right) \\ \times (D_{11})_3 \frac{\partial^3 y_3}{\partial x^3} + (B_{11})_3 \frac{\partial^2 u_3}{\partial x^2} - \frac{wh_3 G}{4h_0} \\ \times \left(2 \frac{\partial u_2}{\partial x} - 2 \frac{\partial u_3}{\partial x} + h_2 \frac{\partial^2 y_2}{\partial x^2} + h_3 \frac{\partial^2 y_3}{\partial x^2} \right). \end{aligned} \tag{65}$$

Moment balance:

$$\begin{aligned} (B_{11})_1 \frac{\partial u_1}{\partial x} + (D_{11})_1 \frac{\partial^2 y_1}{\partial x^2} = (B_{11})_2 \frac{\partial u_2}{\partial x} \\ + (D_{11})_2 \frac{\partial^2 y_2}{\partial x^2} + (B_{11})_3 \frac{\partial u_3}{\partial x} + (D_{11})_3 \frac{\partial^2 y_3}{\partial x^2} \end{aligned}$$

$$\begin{aligned}
 & - \left[(A_{11})_2 \frac{\partial u_2}{\partial x} - (B_{11})_1 \frac{\partial^2 y_2}{\partial x^2} \right] \left(\frac{h_1 - h_2}{2} \right) \\
 & + \left[(A_{11})_3 \frac{\partial u_3}{\partial x} - (B_{11})_3 \frac{\partial^2 y_3}{\partial x^2} \right] \left(\frac{h_1 - h_3}{2} \right). \quad (66)
 \end{aligned}$$

Force balance in the axial direction:

$$\begin{aligned}
 (A_{11})_1 \frac{\partial u_1}{\partial x} + (B_{11})_1 \frac{\partial^2 y_1}{\partial x^2} &= (A_{11})_2 \frac{\partial u_2}{\partial x} + (B_{11})_2 \frac{\partial^2 y_2}{\partial x^2} \\
 &+ (A_{11})_3 \frac{\partial u_3}{\partial x} + (B_{11})_3 \frac{\partial^2 y_3}{\partial x^2}. \quad (67)
 \end{aligned}$$

The continuity conditions between Regions 2 and 4 at $x = l_1 + l_2$ are similar to Eqs. (59–67) and are not presented for the sake of brevity.

at $x = L$:

$$\text{Shear load} = F(t) : (B_{11})_1 \frac{\partial^2 u_1}{\partial x^2} + (D_{11})_1 \frac{\partial^3 y_1}{\partial x^3} = F(t). \quad (68)$$

$$\text{Moment} = 0 : (B_{11})_1 \frac{\partial u_1}{\partial x} + (D_{11})_1 \frac{\partial^2 y_1}{\partial x^2} = 0. \quad (69)$$

$$\text{Axial load} = 0 : (A_{11})_1 \frac{\partial u_1}{\partial x} + (B_{11})_1 \frac{\partial^2 y_1}{\partial x^2} = 0. \quad (70)$$

3. Experimental investigations

3.1. Material

Unidirectional composite plates with thickness of 5 mm were manufactured from E-glass/epoxy composite material with a ply thickness of 0.125 mm. Sixteen-layer patches with ply angles of 0° and 90° (measured from the direction of the beam) were manufactured from material similar to the composite beams. Furthermore, patches with the stacking sequence of [45°/-45°]₃ were manufactured from fiberglass/epoxy composite with S glass fibers and ply thickness of 0.3 mm. The composite plates were cured at 120 °C and 180 kPa for 1 h, and then were air-cooled under constant pressure. The cured composite plates were then cut into specimens of 25.4 mm in width. Damage sections of various sizes and locations were introduced by removal of sections from the composite beams with a milling machine. Fig. 3 depicts a specimen before and after machining. Table 1 shows the list of the manufactured composite patches and their corresponding numbers of plies. Specimens 1–5 were repaired with patches manufactured from the parent



Fig. 3. The manufactured composite beams, before and after machining, and with a repair patch.

Table 1
Patch stacking sequence and its location in the manufactured repaired composite beam specimens

Specimen no.	Patch stacking sequence	l_2 (cm)
1		0
2	[0] ₁₆	7.62
3	[90] ₁₆	2.54
4	[90] ₁₆	5.08
5	[90] ₁₆	7.62
6	[45/-45] ₄	5.08
7	[45/-45] ₄	7.62
8	[45/-45] ₄	10.16
9	[45/-45] ₄	15.24

Table 2
Mechanical properties of E-glass/epoxy and fiberglass/epoxy composites measured utilizing ultrasonic method

Composite	Fiber direction	Transverse to fiber direction
E-glass/epoxy	53.0 Gpa	17.65 GPa
Fiberglass/epoxy	38.80 GPa	14.50 GPa

beam material (E-glass/epoxy), while specimens 6–9 were patched with fiberglass/epoxy composite with S glass fibers. Ultrasonic testing was conducted in order to evaluate the elastic moduli of the fiberglass/epoxy with and E-glass/epoxy in the direction of the fiber and transverse to it. The results presented in Table 2 are the mean values from three different composite specimens. These values are within 10% of the values reported by the manufacturer.

The surface of the beam and patch in the bond area were sand blasted and cleaned with acetone prior to repair of the machined sections. Repair patches were bonded to the composite beam with an epoxy having density of 1.15 g/cm³. The elastic modulus of the

adhesive was evaluated by means of an ultrasonic method to be $E_a = 5.3 \text{ GPa}$. The adhesively bonded joints were cured at 120°C for 30 min and then were air-cooled under constant pressure. Fig. 3 depicts the repaired composites with the adhesively bonded fiberglass/epoxy composite patch. The length of each repaired composite beam is 305 cm and the repair patch is located at the middle of the beam.

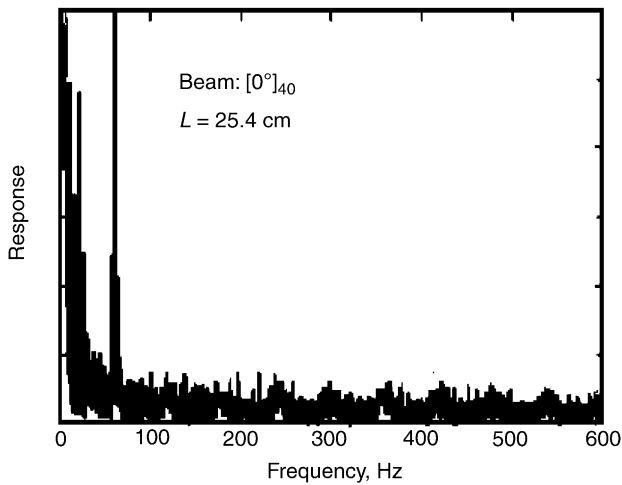


Fig. 4. A typical frequency spectrum of a composite beam with no damage, obtained by striking the beam with a wooden hammer at its free end and measuring the transverse dynamic response at its free end with a non-contact, laser doppler vibrometer.

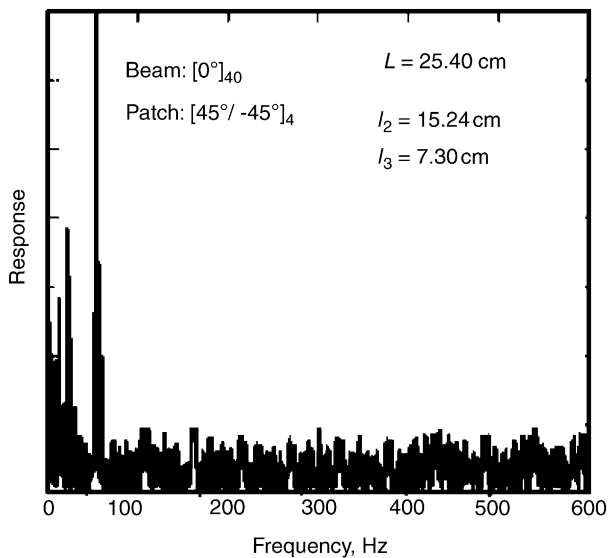


Fig. 5. A typical frequency spectrum of a repaired composite beam, obtained by striking the beam with a wooden hammer at its free end and measuring the transverse dynamic response at its free end with a non-contact, laser doppler vibrometer.

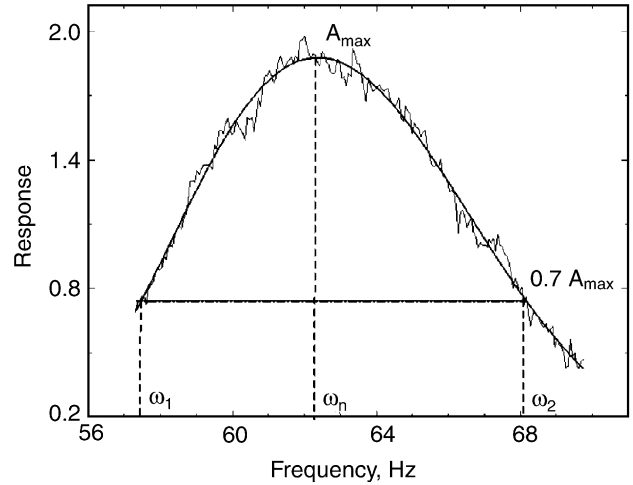


Fig. 6. A portion of a frequency response used to evaluate the damping ratio ζ .

3.2. Dynamic response measurement

The dynamic response of the repaired composite beams was obtained by clamping one end of the beam to a heavy stone table and striking the beam with a wooden hammer at its free end. A non-contact, laser doppler vibrometer was utilized to record the transverse dynamic response of the composite beam at a point near its free end. No attempt was made to measure the axial dynamic response of the beams. Figs. 4 and 5 present typical frequency responses of beams with and without the repair patch. The peak response frequencies were identified from the peaks in the frequency spectra. In addition, the system damping ratio was evaluated from the quality factor Q from ω_1 and ω_2 corresponding to half-power (Fig. 6).

$$Q \approx \frac{1}{2\zeta} \approx \frac{\omega_n}{\omega_2 - \omega_1} \tag{71}$$

A Matlab program was developed to assess the best fit to the frequency spectrum from which maximum amplitude and half-power points were obtained. The experimental results for the first peak response frequency and damping ratio for each repaired beam are presented in Table 3. Each experimental data point is the mean value from at least three experiments. Furthermore, the effects of total specimen length and patch location on dynamic response of the repaired beams were investigated by changing the location of the clamping device (Table 3).

4. Results and discussions

Matlab-based codes were developed to analyze the dynamic response of the repaired composite beam under

Table 3

The first peak response frequencies and their corresponding modal damping ratios for the manufactured repaired composite beam specimens

Specimen no.	l_2 (cm)	Stacking sequence	$L = 20.32$ cm		$L = 22.86$ cm		$L = 25.4$ cm	
			f_1 (Hz)	ζ	f_1 (Hz)	ζ	f_1 (Hz)	ζ
1	0		92.81	0.00336	73.12	0.00434	60	0.00460
2	7.62	[0] ₁₆	82.34	0.00396	65.00	0.00524	54.53	0.00571
3	2.54	[90] ₁₆	83.44	0.00377	68.75	0.00452	55.16	0.00477
4	5.08	[90] ₁₆	74.30	0.00415	62.97	0.00522	53.90	0.00584
5	7.62	[90] ₁₆	65.16	0.00476	58.44	0.00561	48.60	0.00787
6	5.08	[45/-45] ₄	86.25	0.00380	69.69	0.00451	57.97	0.00519
7	7.62	[45/-45] ₄	84.14	0.00335	67.95	0.00460	56.79	0.00574
8	10.16	[45/-45] ₄	78.44	0.00460	66.25	0.00484	56.72	0.00588
9	15.24	[45/-45] ₄	67.34	0.00485	62.03	0.00531	54.06	0.00600

a harmonic peeling load based on the proposed theoretical investigations presented in Section 2. The analyses were performed for composite beams of similar geometries and material properties. Since there are no data available on the adhesive loss factor, it was taken as a variable and its effect on the system response was investigated. No attempt was made to measure the actual adhesive loss factor.

4.1. Dynamic response of repaired composite beams

Figs. 7 and 8 present the transverse and axial frequency responses of the repaired composite beam at the location of the applied force (free end) for specimen No. 3 ($L = 25.4$ cm) with various adhesive loss factors. The results indicate that there is apparently no correlation between the theoretical and experimental results, Table 3, for the corresponding specimen geometries and properties. For example, the proposed theoretical model predicts the first peak response frequency of specimen no. 3 ($L = 25.4$ cm) to be 215 Hz, in contrast with the 55 Hz from the experimental investigations. Similar discrepancies were also revealed between the theoretical and experimental results for the other specimens.

In order to explore the shortcomings of the proposed theoretical investigations, finite element modal analysis was performed with ANSYS. The finite element model employed 3676 eight-node shell elements with the same material properties and geometry as specimen no. 3. The adherends and the patch were modeled as anisotropic material while the adhesive layer was modeled as a linear elastic material. Mesh sensitivity analysis was performed and it was concluded that further refinement of the mesh does not change the results of the modal analysis significantly. Based on the results of the finite element analyses, the first resonant frequency of the repaired composite beam is 55.4 Hz, which is in good agreement with the experimental results. In addition, modeling of the repaired section of the beam as the multilayer laminated beam and use of the classical composite beam

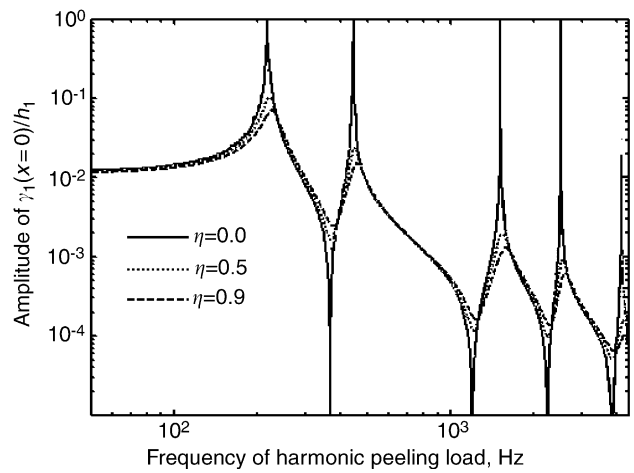


Fig. 7. The results of the theoretical model for the transverse frequency response of the repaired composite beam (specimen no. 3) at its free end with various adhesive loss factors subject to 1 N harmonic peeling load applied at its free end.

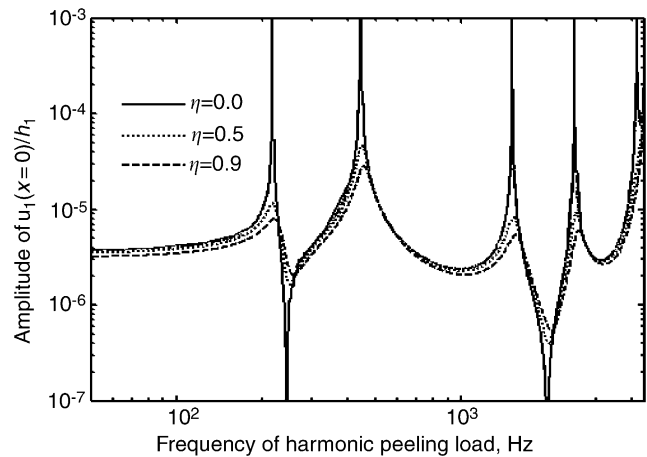


Fig. 8. The results of the theoretical model for the axial frequency response of the repaired composite beam (specimen no. 3) at its free end with various adhesive loss factors subject to 1 N harmonic peeling load applied at its free end.

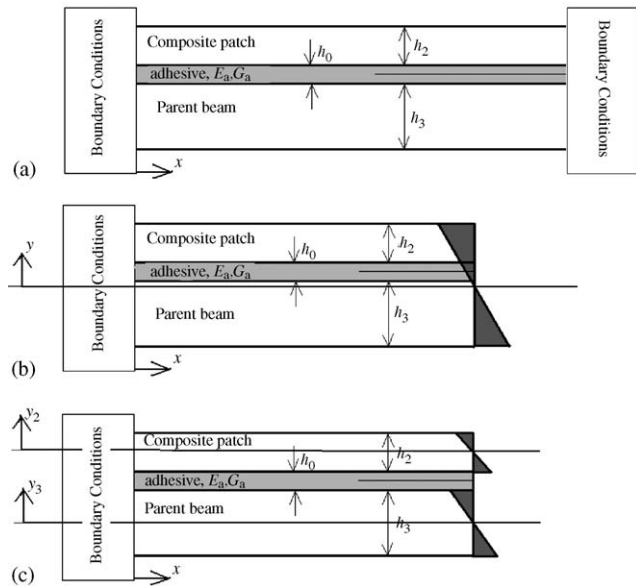


Fig. 9. The deformation fields of the repair section with adhesive having (b) a low value of elastic modulus (the shear deformation is the dominant mechanism of deformation) and (c) a high value of elastic modulus (the beam acts as a classical composite beam).

theory led to a prediction of 55.8 Hz for the first natural frequency of the repaired composite, which is again in good agreement with both experimental and finite element analysis results. Fig. 9 depicts the difference between the displacement fields assumed in the theoretical investigation (Fig. 9b) and in the classical composite beam theory (Fig. 9c).

Finite element analyses were performed for a range of adhesive elastic modulus values for the geometry and material properties corresponding to specimen no. 2 ($L = 25.4\text{ cm}$) in order to gain some insight into the effect of adhesive elastic modulus on the dominant deformation mechanism and the vibration characteristics of the repaired composite beam. The adhesive elastic modulus was normalized by the parent beam (E-glass/epoxy) elastic modulus in the fiber direction, E_a/E_{long} . Furthermore, the dimensionless resonant frequency of the repaired composite beam was defined as ψ_n (the n th resonant frequency of the repaired composite beam/ the n th resonant frequency of the parent composite beam with the same geometrical parameters and mechanical properties). Figs. 10 and 11 present the 1st and 2nd dimensionless resonant frequencies of the repaired composite for various adhesive elastic moduli, based on the model proposed in the theoretical investigations, the classical composite beam theory, and finite element analyses. For the composite beam geometry and material properties studied, the presence of the repair could decrease the first resonant frequency of the repaired beam by about 78% (for very low elastic modulus of adhesive). For high elastic modulus of

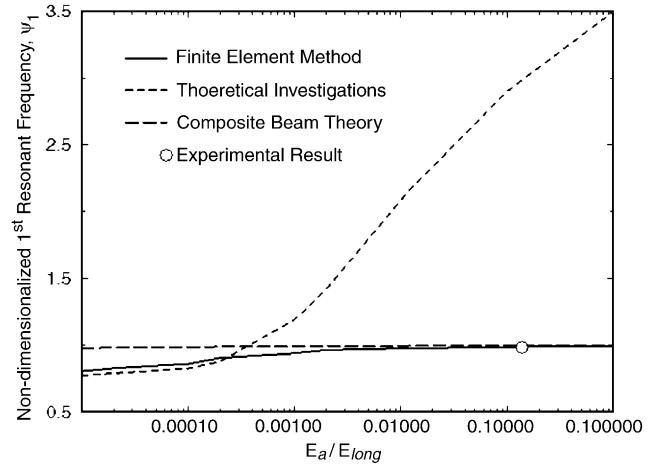


Fig. 10. The 1st normalized resonant frequency of the repaired composite versus dimensionless elastic modulus of the adhesive, based on the theoretical model, composite beam theory, and finite element analysis. (The adhesive elastic modulus is normalized with respect to the parent beam (E-glass/epoxy) elastic modulus in the fiber direction).

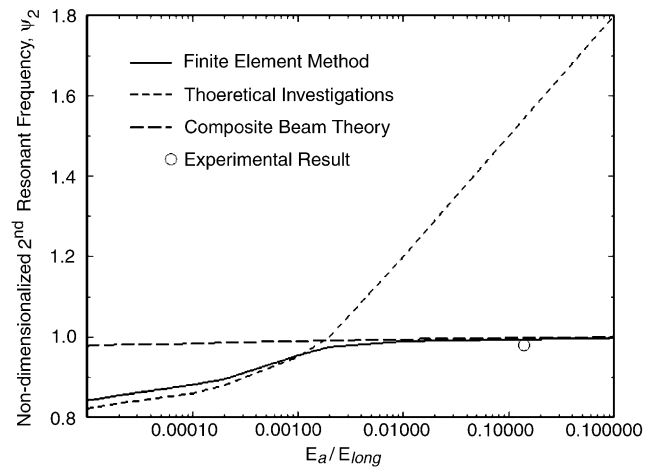


Fig. 11. The 2nd normalized resonant frequency of the repaired composite versus dimensionless elastic modulus of the adhesive, based on the theoretical model, composite beam theory, and finite element analysis. (The adhesive elastic modulus is normalized with respect to the parent beam (E-glass/epoxy) elastic modulus in the fiber direction).

adhesive, $E_a/E_{long} > 0.05$, the resonant frequencies of the repaired composite beam did not exhibit significant sensitivity to the adhesive elastic modulus. In contrast, for low elastic modulus of the adhesive, the repaired composite beam resonant frequencies were significantly sensitive to the adhesive elastic modulus. In addition, the 2nd resonant frequency of the repaired composite beam exhibited lower sensitivity to the adhesive elastic modulus than its 1st resonant frequency. For example, for the lowest normalized adhesive elastic modulus depicted in Figs. 10 and 11, $\psi_1 \approx 0.78$, while $\psi_2 \approx 0.84$. This can be justified by considering the mode shapes of

the repaired composite beam. In addition, the finite element results indicate that the dominant mechanism of deformation of the adhesive layer depends significantly on the relative elastic modulus of the adhesive. For a very low adhesive elastic modulus, the results of the proposed theory replicate results of finite element analysis, as the adhesive layer shear deformation is the dominant mechanism. However, for high elastic modulus of the adhesive, results of finite element analysis diverge from the results of the theoretical investigations and approach the results of the classical composite beam theory, indicating a transition to the bending deformation of the total cross section. It should be noted that, for moderate adhesive elastic modulus, the mechanism of deformation is based on combination of the shear deformation in the adhesive layer and bending deformation of the total cross section. In this range of adhesive elastic modulus, none of the proposed theories result in an acceptable estimation of the resonant frequencies of the repaired composite beam. For example, for the results presented in Fig. 10, this range for the adhesive elastic modulus can be identified as $0.0002 < E_a/E_{\text{long}} < 0.005$. A model that can represent the deformation mechanism of the adhesive layer more accurately should be developed for this range of adhesive elastic modulus.

The modal finite element analyses of the repaired composite beam indicated that, for moderate and high elastic modulus of adhesive, the first three mode shapes of the repaired composite beams were not significantly different from these of the parent beam. However, higher mode shapes might be significantly affected by the presence of the repair patch.

4.2. Damping ratio of repaired composite beams

The modal damping ratio of the repaired composites was predicted from the experimental results. The details of the experimental investigations were presented in Section 3. Table 3 presents the effects of various patch sizes and stacking sequences on the modal damping ratios corresponding to the first peak response frequency of the repaired composite beam. The results indicate that increasing the length of the composite beam increases the modal damping. This could be related to the composite material viscosity. Furthermore, by comparing the modal damping of specimens no. 1 and 2, it can be concluded that repairing the composite beam with the same material and stacking sequence, as that of the parent material does not change the damping characteristics of the system significantly. This can be explicated by considering the deformation field in the repair region, Fig. 9b. Although adhesive has a high-energy loss in the shear, it undergoes little shear deformation because of its high elastic modulus. The effects of adhesive energy loss should be more pro-

nounced for an adhesive with low elastic modulus. In addition, the results presented in Table 3 show that repairing the composite having $[90]_{16}$ stacking sequence increased the modal damping ratio of the repaired composite beam. This can be explained by considering that the composite has greater energy loss in the direction normal to the fiber direction.

5. Concluding remarks

The dynamic response of repaired composite beams with an adhesively bonded patch was investigated theoretically and experimentally. In the theoretical part, the equations of motion of the composite beam with an adhesively bonded repair patch were derived assuming that the adhesive layer resists both shear and peeling stresses and both the patch and based materials behave as Euler–Bernoulli beams. To assess the validity of the proposed theoretical model, the results of the theoretical model were compared with those obtained from the finite element analysis. The outcome of the comparative study suggested that the elastic modulus of the adhesive layer dominates the mechanism of deformation of the repaired beam and its vibration characteristics. For very low values of adhesive elastic modulus, the adhesive layer deforms under shear and the theoretical model replicated the results of the finite element analysis. In contrast, for high values of adhesive elastic modulus, the results obtained by using the classical composite beam theory were in good agreement with those of the finite element analysis, while the proposed theoretical model significantly underestimated the resonant frequencies of the repaired composite beam. Theoretical results indicate that the proper modeling of adhesive behavior is important in model analyses of the repaired composites.

In the experimental investigation, the vibration characteristics of the unidirectional fiberglass-reinforced epoxy composite specimens with various repaired patches were obtained by hammer test technique using a non-contact laser vibrometer. Finite element analysis and the classical composite beam theory predicted the first resonant frequency of the composite beams accurately. A limited results on the effect of the patch material properties, stacking sequence and length on the vibration characteristics of the composite beam was presented.

References

- [1] Nayeb-Hashemi H, Harrison A, Vaziri A. Dynamic response of a heat damaged fiber-resin beam subjected to harmonic forcing at the tip. *J Compos Technol Res* 2003;25(2):87–95.
- [2] Pai FP, Naghshineh-Pour AH, Schulz MJ, Chung J. Dynamic characteristics and buckling strength of composite-repaired aluminum plates. *Finite Element Anal Des* 1998;28:255–75.

- [3] Bary SM, Loader CB, Hawyes VJ, Humberstone L, Curtis PT. A smart repair system for polymer matrix composites. *Composite, Part A: Appl Sci Manuf* 2001;32:1767–76.
- [4] Charalambides MN, Hardouin R, Kinloch AJ, Matthews FL. Adhesively bonded repairs to fiber-composite materials. I: experimental, *Composites, Part A: Appl Sci Manuf* 1998;29(11):1371–81.
- [5] Jones R, Bartholomeusz R, Kaye R, Roberts J. Bonded-composite repair of representative multi-site damage in a full-scale fatigue-test. *Theor Appl Fract Mech* 1994;21:41–9.
- [6] Paul J, Jones R. Repair of impact damaged composites. *Eng Fract Mech* 1992;41(1):127–41.
- [7] Dehm S, Wurzel D. Fast, in-situ repair of aircraft panel components. *J Aircraft* 1989;26(5):476–81.
- [8] Baker AA. Repair of cracked or defective metallic aircraft components with advanced fiber composites—an overview of Australian work. *Compos Struct* 1984;2(2):153–81.
- [9] Hart-Smith LJ. The design of repairable advanced composite structures. Douglas Paper 7550. Presented to SAE aerospace technology Conference, 14–17 October 1985.
- [10] Kurachi EA, Hart-Smith LJ. Design details for adhesively bonded repairs of fibrous composite structures. Douglas Paper 7637, Presented to 31st national sample symposium and exhibition, 8–10 April 1986.
- [11] Nayeb-Hashemi H, Jawad OC. Theoretical and experimental evaluation of the bond strength under peeling loads. *J Eng Mater Technol* 1997;119(4):415–21.
- [12] Olia M, Rossettos JN. Analysis of adhesively bonded joints with gaps subjected to bending. *Int J Solids Struct* 1999;33:2681–93.
- [13] Rossettos JN, Lin P, Nayeb-Hashemi H. Comparison of the effects of debonds and voids in adhesive joints. *J Eng Mater Technol* 1994;116:533–8.
- [14] Apalak MK, Engin A. Geometrically non-linear analysis of adhesively bonded double containment cantilever joints. *J Adhes Sci Technol* 1997;11(9):1153–95.
- [15] Sato C, Ikemagi K. Dynamic deformation of lap joints and scarf joints under impact loads. *International Journal of Adhesion and Adhesives* 2000;20(1):17–25.
- [16] He S, Rao MD. Vibration analysis of adhesively bonded lap joint., Part I: Theory. *J Sound Vib* 1992;152(3):405–16.
- [17] Rao MD, He S. Vibration analysis of adhesively bonded lap joint, Part II: numerical solution. *J Sound Vib* 1992;152(3):417–25.
- [18] Mahadesh KA, Hakeem SA. Optimum design of symmetric composite patch repair to center cracked metallic sheet. *Compos Struct* 2000;49(3):285–92.
- [19] Jones R, Chiu WK. Composite repairs to cracks in thick metallic components. *Compos Struct* 1999;44(1):17–29.
- [20] Naboulsi S, Mall S. Nonlinear analysis of bonded composite patch repair of cracked aluminum panels. *Compos Struct* 1998;41(3–4):303–13.
- [21] Chalkley P, Baker AA. Development of a generic repair joint for certification of bonded composite repairs. *Int J Adhes Adhes* 1999;19:121–32.
- [22] Rastogi N, Soni SR, Denney JJ. Analysis of bonded composite patch repaired metallic structures: An overview. *Structural dynamics and Materials Conference*, 1998. p. 1578–88.
- [23] Kocher LH, Cross SL. Reinforced cutouts in graphite composite structures. ASTM-STP-497, 1972. p. 382–95.
- [24] Jones R, Callinan RJ, Agarwal KC. Stress analysis of adhesively bonded repairs to fiber composite structures. Structures report 386. 2nd ed. Aeronautical Research Laboratories, Australia.
- [25] Li G, Pourmohamadian N, Cygan A, Peck J, Helms JE, Pang SS. Fast repair of laminated beams using UV curing composites. *Compos Struct* 2003;60(1):73–81.
- [26] Charalambides MN, Kinloch AJ, Matthews FL. Adhesively bonded repairs to fiber-composite materials, II: finite element modeling. *Composites, Part A: Appl Sci Manuf* 1998;29(11):1383–96.
- [27] Laura PAA, Cutierrez RH, Rossi RE, Rossit CA, editors. Transverse vibrations of a clamped rectangular plate or slab with an orthotropic patch. *J Sound Vib (Letters to the editor)* 2000;238(4):705–9.
- [28] Vaziri A, Hamidzadeh HR, Nayeb-Hashemi H. Dynamic response of adhesively bonded single-lap joints with a void subjected to harmonic peeling loads. *J Multibody Dynamics* 2001;215(4):199–206.
- [29] Vaziri A, Nayeb-Hahsemi H. Dynamic response of the tubular joint with an annular void subjected to a harmonic torsional loading. *J Multibody Dynamics* 2002;216(4):361–70.
- [30] Vaziri A, Nayeb-Hahsemi H. Dynamic response of the tubular joint with an annular void subjected to a harmonic axial loading. *Int J Adhes and Adhesives* 2002;22:367–73.
- [31] Vaziri A, Nayeb-Hashemi H, Hamidzadeh HR. Experimental and analytical investigation of the dynamic response of a lap joint subjected to harmonic peeling loads. *J Vibrat Acoust* 2004;126(1):84–91.